Chapter 5

Verification of Finite Volume Computations on Steady State Fluid Flow and Heat Transfer

Main contents of this chapter are published as:
J. Cadafalch, C.D. Pérez-Segarra, R. Còsul and A. Oliva. Verification of Finite Volume Computations on Steady State Fluid Flow and Heat Transfer. *Journal of Fluids Engineering*, 124:11-21, March 2002.

Abstract. This work presents a post-processing tool for the verification of steady state fluid flow and heat transfer finite volume computations. It is based both on the generalised Richardson extrapolation and the Grid Convergence Index (GCI). The observed order of accuracy and a error band where the grid independent solution is expected to be contained are estimated. The results corresponding to the following two and three dimensional steady state simulations are post processed: a flow inside a cavity with moving top wall, an axisymmetric turbulent flow through a compressor valve, a premixed methane/air laminar flat flame on a perforated burner and the heat transfer from an isothermal cylinder enclosed by a square duct. Discussion is carried out about the certainty of the estimators obtained with the post-processing procedure. They have been shown to be useful parameters in order to assess credibility and quality to the reported numerical solutions.

5.1 Introduction

During the last decades the numerical methods on heat transfer and fluid flow have been consolidated as an indispensable tool for the resolution of thermal and mechanical engineering problems, being nowadays an essential complement to the experimental studies. The aim of the Computational Fluid Dynamics (CFD) scientific community up to the last years was mainly focussed on improving the performance of the numerical methods in order to increase the range of applications, i.e. larger domains and more and more complex physical phenomena. As a result, many commercial codes have appeared on the market and are being used by many engineers and technicians in their projects and companies for design, evaluation and testing of new equipment and even entire systems (virtual prototyping and virtual testing), decreasing dramatically the time and cost of bringing new products to the market. Together with the increase of the number of users on these techniques, a discussion about the need of assessing the credibility of the numerical results has emerged in the scientific Computational Fluid Dynamics community. Prestigious journals and institutes in the field of CFD and heat transfer have adopted statement policies about this subject [1][2], and many papers have been published concerning the quantification of the numerical errors and the quality of the numerical solutions [3][4].

A numerical solution is the final result of two steps: a modeling of the physical phenomena so as to obtain a set of PDEs (physical or mathematical model), and the conversion of these PDEs to algebraic equations and their solution on a computer (computational model). The first step concerns modeling research such as turbulence modeling and modeling of chemical kinetics. The second step involves the discretization of the PDEs, the numerical procedures to solve the algebraic equations, the programming of the code, the criteria for finishing the convergence procedure and the computer accuracy. Both steps introduce approximations in the solutions, and the resulting errors should be independently understood and quantified, if possible. The errors introduced in the second step are known as computational errors and the process to study these errors as verification process. Once the mathematical model and the computational model have been independently verified, the final validation of the simulation process should be carried out by comparing the results predicted by the simulation with experimental data, which is known as validation process. In this context, validation process is the last step of the overall procedure required to assess credibility. Furthermore, in validation processes, uncertainties arise in both the experimental results and the computational results. Therefore, when analyzing discrepancies between simulation and experimental data attention must be focussed not only on the numerical solution (mathematical model and computational model), but also on the procedure adopted to obtain the experimental data. Fer example, experimental uncertainties can come about when testing is done under conditions other than the operating conditions of the studied system or equipment.

From the different processes involved to assess the credibility of fluid dynamics and heat transfer computations (the study of the physical model, the verification and the validation), this work focuses on the verification process. The main source of computational errors is the discretization. In steady state problems, using double precision real numbers with strong enough convergence criteria, and when the code is free of programming errors and bugs, the remaining computational error is caused by the geometric discretization (mesh) and the numerical discretization (numerical scheme). In order to quantify these errors, two different parameters are usually adopted: h, which is representative of the mesh spacing, and p, which stands for the order of accuracy of the numerical scheme. The h-refinement treatment is commonly used to reduce the grid discretization errors in finite volume techniques (i.e. the numerical scheme is fixed and the mesh is refined). In these studies, the Richardson extrapolation can be adopted as a formally upper-order extrapolated solution estimator and as an error estimator [5].

The goal of this work is to show the capability of a post-processing tool for the computational error analysis of the simulations of different kind of steady state flows and physical phenomena: laminar flows, turbulent flows using two equations turbulence models [6] and reactive flows [7]. The studies are based on the generalized Richardson extrapolation for h-refinement studies and on the Grid Convergence Index (GCI) proposed by Roache [8]. First results using this tool for steady state laminar and turbulent flows have already been reported by the authors [9][10].

The post-processing procedure here described, has been designed so as to establish criteria about the sensitivity of the simulation to the computational model parameters that account for the discretization: the mesh spacing and the order of accuracy. For transient calculations, not considered here, an additional parameter should be added in order to account for the order of accuracy of the time-marching scheme. This tool estimates the order of accuracy of the numerical solution (observed order of accuracy) and a error band where the grid independent solution is expected to be contained (uncertainty due to discretization), also giving criteria about the credibility of these estimations. Both global estimators and local estimators are calculated. Local estimators make it possible to find out local source of error such as zones with inadequate mesh concentration or problems with an inadequate formulation of the boundary conditions. Therefore, they are very useful to improve the numerical solutions. However, as they consist of a large amount of data such as maps of observed order of accuracy or maps of estimated local discretization error, they seem to give too much information and usually not clear enough, for the final reporting of the results. For such purposes, the global estimators are easier to be used and reproduced for different authors in different reports.

To show the capability of these tools, different results of two and three dimensional steady state problems solved on a h-refinement criteria have been post processed: a

flow inside a cavity with moving top wall, an axisymmetric turbulent flow through a compressor valve, a premixed methane/air laminar flat flame on a perforated burner and the heat transfer from an isothermal cylinder enclosed by a square duct. Both structured rectangular or axisymmetric staggered grids, and body fitted non-staggered grids are used. A solution with a very fine grid and high order numerical scheme has been calculated for all the tested cases and it has been considered the "exact" or reference solution. With this "exact" solution, the "exact" errors of the numerical solutions have been calculated and compared to the uncertainty obtained from the post-processing tool. The values of the global estimators are given for all the post processed cases together with the "exact" absolute error. The values of some local estimators for one of the cases are also given and discussed.

So as to point out the credibility of the estimators obtained with the post processing tool, a simple case with analytical solution has been solved numerically using an h-refinement criteria. The uncertainty due to discretization calculated from the post-processing has been compared to the real discretization error obtained from the comparison of the numerical solution to the analytical solution.

In the following section an overview of the mathematical basis on the evaluation of discretization errors is given. In section 3 details of the post-processing tool are described. The test problems and the mesh used in each of them are explained in section 4. Finally, the results are given and discussed in section 5.

5.2 Fundamentals

5.2.1 Estimation of the discretization errors: Mathematical formulation

Assuming that the numerical solution of a problem is free of convergence errors, round-off errors and programming errors, the computational error at a given point $\mathbf{x}$ of the computational domain is only due to the discretization process. Therefore, the absolute error due to discretization can be defined as the absolute difference between the computed solution $\phi(\mathbf{x})$ and the exact solution $\phi_E(\mathbf{x})$:

$$e_D(\mathbf{x}) =\mid \phi(\mathbf{x}) - \phi_E(\mathbf{x}) \mid \tag{5.1}$$

As in practical situations the exact solution or an estimation of the exact solution is not available, the discretization error cannot be calculated using Eq. (5.1). In this section, it is shown how the magnitude of the discretization error can be estimated by means of the Richardson extrapolation theory [5] and the concept of Grid Convergence Index (GCI) for uniform reporting of grid refinement studies [4].

In steady state computations, there are two discretization error sources: the mesh and the numerical schemes. In order to quantify each of them, two parameters of the computational model are usually adopted:

h : geometric discretization parameter representative of the mesh spacing
p : order of accuracy of the numerical schemes

According to the Richardson extrapolation theory, at a given point $\mathbf{x}$ of the domain and when the solution is in the asymptotic range (sufficient small h), the local absolute discretization error can be expressed in terms of the above mentioned parameters and of a coefficient $C_p(\mathbf{x})$ [5]:

$$e_D(\mathbf{x}) =\mid C_p(\mathbf{x})h^p \mid \tag{5.2}$$

With three solutions of a problem ($\phi_1(\mathbf{x})$, $\phi_2(\mathbf{x})$ and $\phi_3(\mathbf{x})$) obtained by means of a h-refinement treatment on the grids $h_1 = h$ (fine grid), $h_2 = rh$ (middle grid), and $h_3 = r^2h$ (coarse grid), a three-equation system of the unknown variables $p(\mathbf{x})$, $\phi_E(\mathbf{x})$, and $C_p(\mathbf{x})$ can be posed:

$$e_{Di}(\mathbf{x}) =\mid \phi_i(\mathbf{x}) - \phi_E(\mathbf{x}) \mid=\mid C_p(\mathbf{x})[r^{i-1}h]^{p(\mathbf{x})} \mid \qquad i = 1, 2, 3 \tag{5.3}$$

where the order of accuracy p has been assumed to be dependent on the position $\mathbf{x}$, and r is the refinement ratio.

From Eq. (5.3) it can be determined that:

$$p(\mathbf{x}) = \frac{\ln[(\phi_2(\mathbf{x}) - \phi_3(\mathbf{x}))/(\phi_1(\mathbf{x}) - \phi_2(\mathbf{x}))]}{\ln r} \tag{5.4}$$

$$e_{D_1}(\mathbf{x}) =\mid \phi_1(\mathbf{x}) - \phi_E(\mathbf{x}) \mid=\mid \frac{\phi_1(\mathbf{x}) - \phi_2(\mathbf{x})}{1 - r^{p(\mathbf{x})}} \mid \tag{5.5}$$

where Eq. (5.4) is meaningful only in case of monotonic convergence to the exact numerical solution as the grid is refined.

With this formulation, a formally upper-order extrapolated value of $\phi_E(\mathbf{x})$ can be calculated [8]. However, the use of the extrapolated value of $\phi_E(\mathbf{x})$ is generally not recommended because of its lack of conservation, and because the assumptions involved in its calculation not always apply in practical problems. On the other hand, the estimator of the absolute discretization error, Eq. (5.5), is a good parameter in order to assess credibility to the numerical solution. Roache [4] incorporates a safety

factor F_s into this estimator and defines the Grid Convergence Index (GCI). At a given point $\mathbf{x}$ of the computational domain, the GCI corresponding to the fine grid solution $\phi_1(\mathbf{x})$ takes the following form:

$$GCI_1(\mathbf{x}) = F_s \mid \frac{\phi_1(\mathbf{x}) - \phi_2(\mathbf{x})}{1 - r^{p(\mathbf{x})}} \mid \tag{5.6}$$

In a two-grid convergence study where $p(\mathbf{x})$ must be assumed according to the formal order of accuracy, a conservative value of $F_s = 3$ is recommended. For higher quality studies using three or more grids, as those presented in this work, and where $p(\mathbf{x})$ can be estimated by means of Eq. (5.4), a value of $F_s = 1.25$ appears to be adequately conservative.

5.2.2 Classification of the calculation nodes

As previously estated, Eq. (5.4) can only be used for the estimation of $p(\mathbf{x})$ at those nodes with monotone error convergence. Futhermore, as the argument of the logarithm function is the ratio between the solution changes $(\phi_2(\mathbf{x}) - \phi_3(\mathbf{x}))$ and $(\phi_1(\mathbf{x}) - \phi_2(\mathbf{x}))$, numerical problems can arise when analysing $\phi(\mathbf{x})$ values close to 0 or nodes with both solution changes approaching 0.

It is useful to classify the calculation nodes into three groups according to the following conditions:

$$\begin{aligned} \textit{Richardson node} &: [\phi_2^*(\mathbf{x}) - \phi_3^*(\mathbf{x})] * [\phi_1^*(\mathbf{x}) - \phi_2^*(\mathbf{x})] > C_0 \\ \textit{Converged node} &: \mid [\phi_2^*(\mathbf{x}) - \phi_3^*(\mathbf{x})] * [\phi_1^*(\mathbf{x}) - \phi_2^*(\mathbf{x})] \mid < C_0 \\ \textit{Oscillatory node} &: [\phi_2^*(\mathbf{x}) - \phi_3^*(\mathbf{x})] * [\phi_1^*(\mathbf{x}) - \phi_2^*(\mathbf{x})] < -C_0 \end{aligned} \tag{5.7}$$

where the upper-index * indicates that the solutions have been normalized by means of the maximum absolute $\phi(\mathbf{x})$, and C_0 is a positive coefficient approaching 0 ($C_0 = 10^{-30}$ in this work, where all the computations have been performed using double precision real numbers).

From the numerical point of view, the Richardson nodes can be defined as those nodes where Eq. (5.4) can be calculated. These Richardson nodes do not necessarily fulfill all the requirements for the generalized Richardson extrapolation. In fact, the solution may be outside the assymptotic range (h not small enough).

Formally, the condition of converged nodes is ill-defined because it can also be accomplished by inflection points in the solution where all three solutions cross through the same point, which are abviously not converged nodes. Nevertheless, no relevant effects of these nodes have been observed in the results post-processed by the authors of this work up to now.

5.2.3 The observed order of accuracy as a certainty parameter

The formal or theoretical order of accuracy depends on the accuracy of the numerical schemes used in the inner and boundary nodes for both the diffusive and convective terms. In some cases such as when the numerical scheme is fully first order (upwind differencial scheme) or second order (central differences), the accuracy of these terms is formally known. However, when hybrid schemes such as Power Law are used, the order of accuracy is bounded but not fixed and it depends on the nature of the problem. Furthermore, different schemes are usually used in the evaluation of the diffusive and convective terms. Therefore, it is plausible to expect an overall order of accuracy p bounded by the order of accuracy of the schemes used. For example, a numerical solution obtained with a code using the first order accurate upwind difference scheme for convective terms and second order accurate central differences for the diffusive terms, should have an order of accuracy between 1 and 2.

A global observed p calculated using the procedure explained in the following section contained within the expected limits of the theoretical p (i.e. observed order of accuracy equals the theoretical order of accuracy), indicates that the numerical solution is converging asymptotically observing the assumptions of the Richardson extrapolation. When this condition is satisfied, the corresponding GCI is expected to be reliable.

5.3 Post-processing tool for the evaluation of the discretization errors

The goal of a tool for the evaluation of the discretization error of a numerical solution is to provide a good estimation of the magnitude of the error. If a grid independent solution is available, this error can be easily calculated. Even for those more extended benchmark problems generally only grid-independent global values are available, such as the average Nu or the velocity distribution in a section of a domain. They are useful for code verification but are still limited for a detailed error evaluation. In fact, in most practical problems the grid independent solution is not available, and it is usually far beyond the available solutions in terms of computational requirements. Therefore, a post-processing tool must deal with concepts such as error estimators and extrapolations, and must also give criteria about the certainty of these estimators and extrapolations as well.

The tool here described is based on the mathematical concepts given in the previous section. This tool not only calculates an error band where the grid-independent solution is expected to be contained, but also the order of accuracy of the numerical solution (observed p). Both local and global estimators are given. When analyzing a problem, local estimators give a detailed information to the CFD code users in order

to know where the convergence problems occurs, to find out where more refinement is necessary or to find bugs in the code. However, when reporting the results they seem to give too much information. In this case, global estimators are more useful.

The post-processing procedure is described in the following subsection step by step. All these steps have to be carried out for all the dependent variables of the problem obtaining for each of them a global observed p and GCI, local values $p(\mathbf{x})$ and $GCI(\mathbf{x})$, and a measurement of the deviation of the local values from the global values.

Step 1: Interpolation at the post-processing grid. The discretized solution of three consecutive refinement levels of a h-refinement study with a constant refinement ratio r (fine grid solution $\phi_1(\mathbf{x})$, middle grid solution $\phi_2(\mathbf{x})$, and coarse grid solution $\phi_3(\mathbf{x})$), are interpolated at the main nodes of the grid where the estimators are calculated (the post-processing grid). This aspect is specially relevant when the numerical solution has been obtained on non-staggered grids. Typically, this mesh could be the coarsest one (grid 3). So as not to introduce additional uncertainties in the post processed numerical solution, third order accurate Lagrangian interpolations are used. Second order interpolations could introduce additional inaccuracies in the numerical solutions obtained with high order schemes such as SMART or QUICK. Grids finer than the coarsest are also not recommended because the extrapolations required in this situation could also introduce additional inaccuracies.

Step 2: Classification of the calculation nodes. All the calculation nodes of the post processing grid are classified into Richardson nodes, converged nodes and oscillatory nodes according to the conditions described in Eq. (5.7). The percentage of each type of calculation node is computed. Boundary nodes and the nodes with fixed ϕ value (blocked-off nodes), are not considered as calculation nodes.

Step 3: Calculation of the local observed p. The local observed order of accuracy $p(\mathbf{x})$ is calculated at all the Richardson nodes of the post-processing grid using Eq. (5.4).

Step 4: Calculation of the global observed p. The global observed order of accuracy is estimated by means of the average of the local order of accuracy at the Richardson nodes. The standard deviation of the local values from the mean values is also calculated. The standard deviation of $p(\mathbf{x})$ from the global p can be considered as a measure of how close the solutions are to the asymptotic range, and, therefore, of the credibility of the estimates obtained from the post-processing procedure.

Step 5: Calculation of the local GCI. The local Grid Convergence Index $GCI(\mathbf{x})$ of the fine mesh is calculated at all the Richardson nodes and converged nodes. At the Richardson nodes $GCI(\mathbf{x})$ is calculated by means of Eq. (5.6) using $F_s = 1.25$ and assuming the order of accuracy $p(\mathbf{x})$ in Eq. (5.6) to be equal to the global observed p calculated in Step 4. At the converged nodes the $GCI(\mathbf{x})$ is assumed to be 0.

Step 6: Calculation of the global GCI. The local GCI weighted by the fraction of volume (between each control volume and the overall volume occupied by all the Richardson nodes and converged nodes) is calculated. The volume weighted average value is taken as the estimator of the global GCI. The standard deviation of the local volume weighted $GCI(\mathbf{x})$ is also calculated. If the global GCI is calculated from the statistical moments of the distribution of the local $GCIs$ without weighting them by the fraction of volume, when post-processing locally refined grids unexpected high values of the global GCI are obtained because the local refinement usually coincide with those zones where the discretization error (and thus the GCI) is higher. In these cases, the global $GCIs$ corresponding to different meshes cannot be directly compared. Another way to avoid this problem is to use a uniform post processing grid instead of using the coarse grid of the studied set of solution, which in practical problems may be refined in some zones.

5.4 Tested cases

The cases presented in this section have been chosen so as to show the capability of the post-processing tool described in this paper for the evaluation of the computational error of different kind of flows, using different grids and different numerical schemes. All of them have been solved with a h-refinement criterion using four, five or six different refinement levels with a refinement ratio $r = 2$ (doubling the mesh). Each refinement level is referenced by means of the parameter n which is properly defined for each case. The values of some governing parameters are pointed out: reference values of the dependent variables for the normalization of the results, main features of the mesh and numerical schemes used. More details about the numerical procedure, solvers, boundary conditions and so on have been left out in this work. They can be found in the references.

5.4.1 Case A: Cavity with moving top wall

Laminar forced flow inside a cavity whose top side moves with a uniform velocity in its own plane in the x direction. The main parameters describing the test case are: $Re = 10^2$ and $Re = 10^3$; $reference\ velocity$=*top wall velocity*; $reference\ length$ = *wall length* (L). Several variants have been computed: two-dimensional flows with side walls inclined at an angle θ with respect to the vertical, see Fig. 5.1a, and three-dimensional flow in a cubic cavity, see Fig. 5.1b. The cavity is discretized with a uniform mesh of $n*n$ control volumes on five levels ($n = 10, 20, 40, 80$ and 160) in the two-dimensional variants, see Fig. 5.1a, and with a uniform mesh of $n*n*n$ control volumes on four levels ($n = 10, 20, 40$ and 80) in the three-dimensional variant, see Fig. 5.1b. Diffusive terms are modeled by means of second order central differences

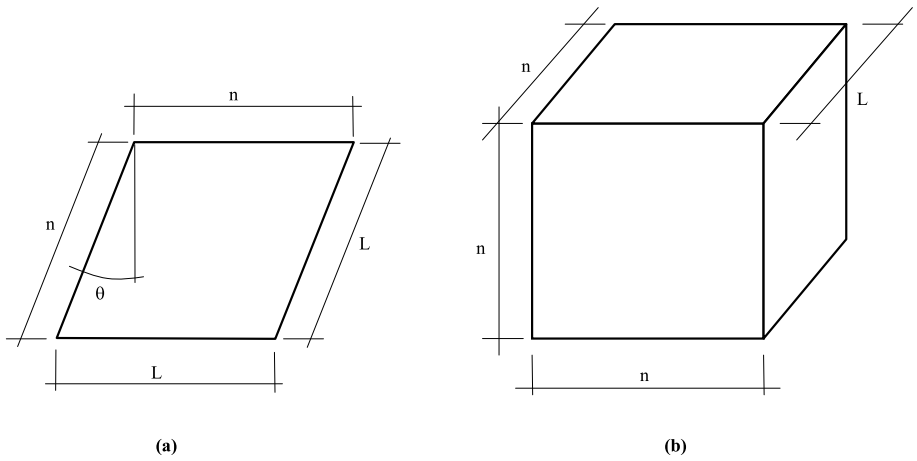

Figure 5.1: Case A: Cavity with moving top wall. (a) Two-dimensional case. (b) Three-dimensional case.

while both the first order accurate UDS scheme (upwind) or the high order accurate SMART scheme are used for the convective terms. For more details see [11][12].

5.4.2 Case B: Axisymmetric turbulent flow through a compressor valve

Modeling of an axisymmetric turbulent flow through an idealized discharge compressor valve by means of low-Reynolds number $k-\epsilon$ turbulence models. The main parameters describing the test case are: $Re = 10^5$; $reference\ velocity$=$average\ velocity\ at\ the\ entrance$ (v_{in}); $reference\ length$=$inlet\ diameter$ (d); $valve\ lift = (s/d)$; $reference\ k = 0.5{v_{in}}^2$; and $reference\ \epsilon = (d/s){v_{in}}^3/d$. The idealized physical domain is described in Fig. 5.2a. It is divided in zones with different number of nodes and with a concentrated grid where necessary (i.e. in the boundary layer close to the solid walls of the inlet port and the radial diffuser), see Fig. 5.2b. A concentration tanh-like function with a concentration factor of 1 has been adopted. Roman numbers from I to XII label the zones. The side of the zones with grid concentration are indicated by a solid triangle, and the number of nodes corresponding to each zone are indicated in terms of the grid parameter n (e.g. when $n = 10$, $40 * 40$, $40 * 10$ and $20 * 10$ control volumes are used in the zones I, III and IV respectively). The h-refinement study is performed with five levels of refinement ($n = 5, 10, 20, 40$ and 80). The post-processing study has been carried out in the zones of interest: the inlet valve port zone and the radial diffuser (zones I, III and IV in Fig. 5.2b). The

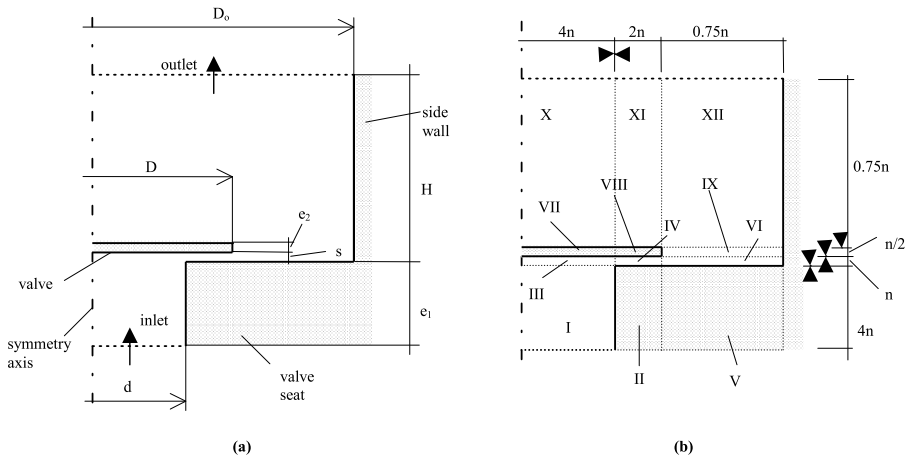

Figure 5.2: Case B: Axisymmetric turbulent flow through a compressor valve. (a) Idealized valve geometry. (b) Mesh and computational domain.

diffusive terms are modeled by means of central differences, the convective terms of the momentum equations with SMART scheme and the convective terms of the additional convection-diffusion equations for the turbulence modeling ($k-\epsilon$) with the Power-Law scheme. See [6][13] for details.

5.4.3 Case C: Premixed methane/air laminar flat flame on a perforated burner

A methane-air homogeneous mixture flows through a drilled burner plate to an open domain. The main parameters describing the test case are: $mass\ flow\ rate = 0.05925 g/cm^2 s$; $inlet\ temperature$=$298.2 K$; $stoichiometric\ mixture$; $reference\ velocity$=$mean\ inlet\ velocity$; $reference\ temperature = inlet\ temperature$; and $reference\ mass\ fractions$=$ten\ per\ cent\ the\ mass\ fractions\ of\ the\ stoichiometric\ combustion$. The burner plate forms a regular pattern of small drilled holes. This plate may be viewed as an ensemble of tiny premixed Bunsen-like burners of a diameter d ordered in a regular honeycomb structure with pitch p. Choosing a small enough diameter and a small enough pitch, the three-dimensional behaviour of the flame is reduced notably adopting a global flat structure disturbed only at the edges of the burner rim and in the vicinity of the drilled holes. Neglecting the effects of the burner rim, the combustion phenomena can be modeled adopting a two-dimensional computational domain enclosed within two symmetry planes, as shown in Fig. 5.3a, accounting for

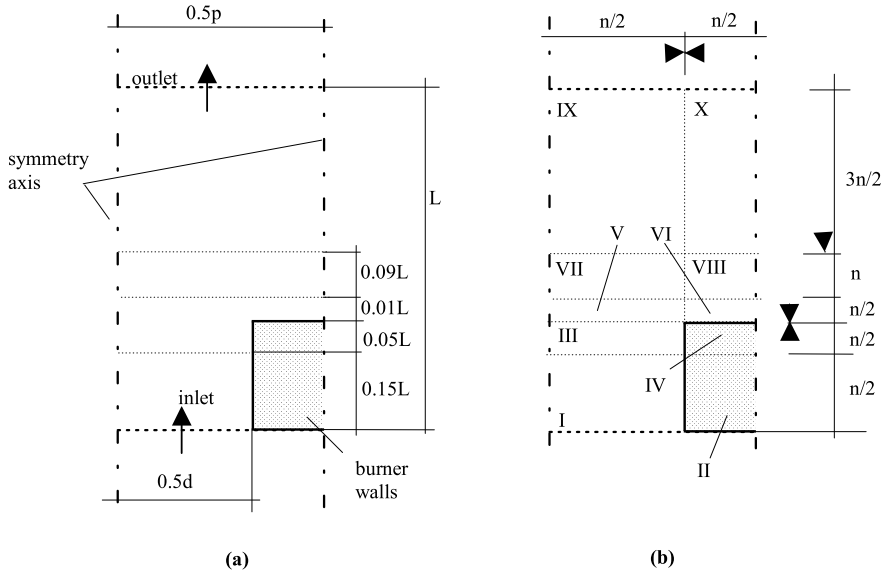

Figure 5.3: Case C: Premixed methane/air laminar flat flame on a perforated burner. (a) Idealized geometry. (b) Mesh and computational domain.

a half burner hole and the corresponding part of the open domain above the burner ($L = 0.4$ cm, $d = 0.03$ cm and $p = 0.045$ cm). The computational domain is divided in zones with different number of nodes and with a concentrated grid where necessary (i.e. near the burner walls and at the flame front) by means of a tanh-like function. The number of grid nodes in each direction and zones is schematically described in Fig. 5.3b. Roman numbers from I to X label the zones. The side of the zones with grid concentration are indicated by a solid triangle, and the number of nodes corresponding to each zone are indicated in terms of the grid parameter n. The h-refinement study is performed with seven levels of refinement ($n = 5, 10, 20, 40, 80, 160$ and 320). This means that when $n = 360$, the domain is discretized with 332.800 control volumes. The post-processing study has been carried out in the zones of interest: flame front (zones III, V, VI, VII and VIII in Fig. 5.3b). The diffusive terms are modeled by means of central differences and both UDS or SMART scheme are used for the convective terms. For details see [6][14][15].

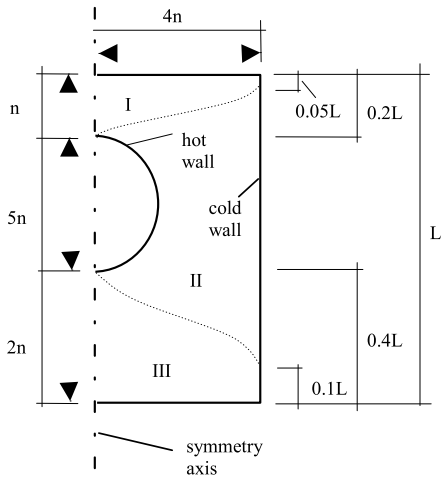

Figure 5.4: Case D: Heat transfer from an isothermal cylinder enclosed by a square duct. Mesh and computational domain.

5.4.4 Case D: Heat transfer from an isothermal cylinder enclosed by a square duct

Heat transfer from a cylinder whose wall is maintained at a constant temperature and is enclosed by an isothermal square duct. The main parameters describing the test case are: $Ra = 10^6$; $Pr = 10$; $reference\ length$=$square\ duct\ side$ (L); $reference\ temperature = reference\ difference\ of\ temperature = cylinder\ temperature - square\ duct\ temperature$ (ΔT); $reference\ velocity = \sqrt{g\beta\Delta TL}$. Details about the geometry and mesh are given in Fig. 5.4. The domain is divided in three different zones. The number of nodes corresponding to each zone is indicated in terms of the grid parameter n. A solid triangle in Fig. 5.4 indicates the zones where the grid has been concentrated by means of a tanh-like function. The domain is discretized using body fitted coordinates with non-staggered grids on five levels of refinement ($n = 2, 4, 8, 16$ and 32). The diffusive terms are modeled by means of central differences, while both UDS or SMART schemes are used for the convective terms. See [6][11][12] for details.

5.5 Results

5.5.1 Description

Calculation of the "exact" computational error.

In order to point out the certainty of the estimators obtained from the post-processing tool, the "exact" computational error has been estimated. To do so, the most accurate solution of each problem (finest mesh with the higher order numerical scheme) has been considered the "exact" solution, $\phi_E(\mathbf{x})$. For each solution i in the h-refinement, the absolute discretization error $e_D(\mathbf{x})$ has been estimated at all the computational nodes of the post-processing grid by means of Eq. (5.1), and finally a global discretization error (e_D) and the standard deviation of the local values have been calculated. The interpolation of the "exact" solution and the solution i at the nodes of the post-processing grid has been performed as indicated in Step 1 of section 5.3, and the global discretization error has been obtained from the local discretization error following the same procedure used for the GCI, see Step 6 of section 5.3 .

Description of the tables of global estimators. For each set of three consecutive meshes on the h-refinement represented by the grid parameter n, the following values are indicated: the percentage of Richardson nodes (Rn), the observed global p, the standard deviation of the local observed $p(\mathbf{x})$ from the global value, the global GCI and the global "exact" absolute discretization error e_D. The upper-index * in the GCI and e_D indicates that they have been normalized using the reference values given in section 5.4 for each of the tested cases (i.e. $GCI^* = GCI/\phi_{ref}$ and $e_D^* = e_D/\phi_{ref}$).

Other data also obtained from the post-processing tool and that have not been included in the tables of global estimators are the percentage of converged nodes and oscillatory nodes, and the standard deviation of the local values of GCI and e_D from the global values. For all the post-processing results presented in this work, the percentage of converged nodes was always 0. Therefore, all those nodes that did not accomplish the condition of Richardson node, Eq. (5.7), were oscillatory nodes. On the other hand, observed deviations of the GCI and e_D in all the cases were of similar magnitude and tended to vanish with the mesh refinement.

For example, table 5.3 shows the global estimators of the three-dimensional driven cavity with moving top wall (case A). As four refinement levels are used in this case, two sets of solutions can be analyzed. For the set of solutions involving the grids $n = 20$, $n = 40$ and $n = 80$ and the numerical scheme UDS, when evaluating the $x - velocity$, 90% of Richardson nodes have been detected. (i.e. 10% of oscillatory nodes). The global order of accuracy of the finest solution of this set ($n = 80$) is 1.2 with a standard deviation of 1.2. The global GCI has a good coincidence with the "exact" absolute error e_D, beeing 0.32 and 0.22 percent of the $x - velocity$ reference value respectively. As the most accurate solution is used as "exact" solution for the

estimation of e_D^*, the e_D^* of these solutions is equal to 0. The cells corresponding to these situations are indicated with a dash (i.e. the set of grids $n = 20$, $n = 40$ and $n = 80$ using the SMART scheme).

5.5.2 Discussion about the tested cases

Case A is a laminar forced flow mainly dominated by internal forces in the inner regions, and the tangential forces at the boundaries. There are no additional source terms that make the convergence with the grid spacing difficult. When solving the Reynolds number $Re = 10^2$, both for the two-dimensional variants (considering two different inclination angles θ) and the three-dimensional variant, even the most coarse meshes seem to belong to the asymptotic range where the generalized Richardson extrapolation can be applied. Therefore, the calculated estimators are expected to be reliable. The global estimators obtained from the post-processing tool are given in tables 5.1 to 5.3.

The results of the variants corresponding to $Re = 10^2$ are given in table 5.1 (two-dimensional flow) and table 5.3 (three-dimensional flow). Specially for the finest meshes, a high percentage of Richardson nodes are computed. The use of the SMART scheme generally increases the number of nodes that converge in an oscillatory manner with the mesh, reducing the number of Richardson nodes. As the flow is dominated by the inertial forces (convective terms), the observed order of accuracy tends to be the one corresponding to the formal order of accuracy of the numerical scheme used for the convective terms (1 in case of UDS, and approximately between 2 and 3 for SMART). The e_D^* are pretty well estimated by GCI^*. The biggest discrepancies are found for the coarsest set of meshes when using the SMART scheme, coinciding with the set of meshes with a lower number of Richardson nodes.

More discrepancies are observed in the variants with $Re = 10^3$ (see table 5.2). With the uniform meshes used, the low-accurate UDS scheme is inappropriate for the case with $\theta = 0$. The observed order of accuracies are significatively lower than the theoretical value of 1 corresponding to this scheme, and they only take values closer to 1 for the finest set of meshes. When using the SMART scheme, observed order of accuracy only differs from the theoretical value for the coarsest set of meshes. The discrepancies between the observed and theoretical values of p for the coarsest meshes indicate that the corresponding estimators of the computational errors are not very reliable. In fact, when comparing the "exact" error to the estimated absolute computational error, differences are observed for the coarsest meshes, which tend to vanish for the higher levels of refinement.

Case B, see table 5.4, is a complex turbulent flow impinging a wall with recirculation zones and zones with a high level of turbulence. Therefore, the results with the coarsest meshes may not be contained in the asymptotic range of convergence. In spite of that, the observed order of accuracy has acceptable values even for the coarse

UDS											
		x-velocity					y-velocity				
grid	θ	Rn	p	$\sigma_{p(x)}$	GCI^*	e_D^*	Rn	p	$\sigma_{p(x)}$	GCI^*	e_D^*
$n_3/n_2/n_1$	$[deg]$	[%]			[%]	[%]	[%]			[%]	[%]
10/20/40		66	1.0	2.4	1.5	.88	77	1.2	1.5	.96	.81
20/40/80	0	89	1.1	1.3	.57	.43	88	1.2	1.3	.47	.39
40/80/160		96	1.1	0.9	.26	.21	96	1.1	0.8	.22	.18
10/20/40		75	1.5	1.4	.76	.52	68	2.0	2.4	.23	.40
20/40/80	60	84	1.5	1.4	.25	.22	84	2.0	1.9	.09	.18
40/80/160		93	1.4	1.0	.12	.08	90	1.5	1.4	.07	.07
SMART											
		x-velocity					y-velocity				
grid	θ	Rn	p	$\sigma_{p(x)}$	GCI^*	e_D^*	Rn	p	$\sigma_{p(x)}$	GCI^*	e_D^*
$n_3/n_2/n_1$	$[deg]$	[%]			[%]	[%]	[%]			[%]	[%]
10/20/40		66	1.4	1.9	.76	.21	77	1.6	1.8	.40	.21
20/40/80	0	82	2.4	1.6	.07	.05	83	2.4	1.3	.05	.05
40/80/160		88	2.1	1.4	.02	-	88	2.2	1.4	.02	-
10/20/40		71	1.6	1.7	.64	.27	62	2.1	2.0	.19	.09
20/40/80	60	84	2.0	1.4	.11	.07	82	2.5	1.6	.04	.04
40/80/160		93	1.9	0.8	.03	-	92	2.1	1.0	.02	-

Table 5.1: Case A: Square cavity with moving top wall, Re=100. Post-processing results. Numerical scheme: UDS and SMART for convective terms and central differences for diffusive terms. (For table description see section 5.5.1).

UDS											
		x-velocity					y-velocity				
grid	θ	Rn	p	$\sigma_{p(x)}$	GCI^*	e_D^*	Rn	p	$\sigma_{p(x)}$	GCI^*	e_D^*
$n_3/n_2/n_1$	$[deg]$	[%]			[%]	[%]	[%]			[%]	[%]
10/20/40		84	0.2	1.5	20.	5.3	85	-0.1	1.5	42.	5.4
20/40/80	0	78	0.2	1.5	26.	3.4	91	0.3	1.1	12.	3.3
40/80/160		86	0.7	1.2	3.1	2.0	92	0.8	1.1	2.7	1.9
10/20/40		72	1.6	1.8	1.3	2.4	72	1.8	1.5	.35	1.1
20/40/80	60	82	1.0	1.6	1.6	1.4	80	1.0	1.9	.56	.67
40/80/160		90	1.1	1.3	.71	.78	89	1.1	1.4	.32	.39
SMART											
		x-velocity					y-velocity				
grid	θ	Rn	p	$\sigma_{p(x)}$	GCI^*	e_D^*	Rn	p	$\sigma_{p(x)}$	GCI^*	e_D^*
$n_3/n_2/n_1$	$[deg]$	[%]			[%]	[%]	[%]			[%]	[%]
10/20/40		81	0.9	1.1	3.5	1.3	80	0.4	1.9	11.	1.4
20/40/80	0	66	1.6	1.8	.70	.29	74	1.5	1.8	.71	.31
40/80/160		93	1.9	1.0	.14	-	96	1.9	0.7	.14	-
10/20/40		65	2.1	1.8	.69	.45	55	1.6	2.2	.45	.30
20/40/80	60	75	2.1	1.9	.18	.10	78	2.0	1.7	.09	.07
40/80/160		78	1.9	1.6	.06	-	82	2.2	1.5	.02	-

Table 5.2: Case A: Square cavity with moving top wall, Re=1000. Post-processing results. Numerical scheme: UDS and SMART for convective terms and central differences for diffusive terms. (For table description see section 5.5.1).

UDS										
	x-velocity					y-velocity				
grid	Rn	p	$\sigma_{p(x)}$	GCI^*	e_D^*	Rn	p	$\sigma_{p(x)}$	GCI^*	e_D^*
$n_3/n_2/n_1$	[%]			[%]	[%]	[%]			[%]	[%]
10/20/40	85	1.3	1.3	.58	.49	84	0.9	1.1	1.3	.48
20/40/80	90	1.2	1.2	.32	.22	91	1.1	1.1	.37	.20
	z-velocity									
grid	Rn	p	$\sigma_{p(x)}$	GCI^*	e_D^*					
$n_3/n_2/n_1$	[%]			[%]	[%]					
10/20/40	84	0.7	1.3	.27	.12					
20/40/80	91	0.8	1.0	.11	.06					
SMART										
	x-velocity					y-velocity				
grid	Rn	p	$\sigma_{p(x)}$	GCI^*	e_D^*	Rn	p	$\sigma_{p(x)}$	GCI^*	e_D^*
$n_3/n_2/n_1$	[%]			[%]	[%]	[%]			[%]	[%]
10/20/40	68	1.7	2.3	.30	.14	70	1.3	1.9	.63	.14
20/40/80	90	1.9	1.2	.07	-	87	2.0	1.2	.08	-
	z-velocity									
grid	Rn	p	$\sigma_{p(x)}$	GCI^*	e_D^*					
$n_3/n_2/n_1$	[%]			[%]	[%]					
10/20/40	77	1.2	1.8	.08	.02					
20/40/80	87	1.9	1.3	.01	-					

Table 5.3: Case A: Cubic cavity with moving top wall, Re=100. Post-processing results. Numerical scheme: UDS and SMART for convective terms and central differences for diffusive terms. (For table description see section 5.5.1).

	radial-velocity					axial-velocity				
grid	Rn	p	$\sigma_{p(x)}$	GCI^*	e_D^*	Rn	p	$\sigma_{p(x)}$	GCI^*	e_D^*
$n_3/n_2/n_1$	[%]			[%]	[%]	[%]			[%]	[%]
5/10/20	68	0.8	1.7	8.4	1.1	79	1.3	1.7	.72	.57
10/20/40	70	1.4	1.8	.76	.31	72	1.3	1.6	.35	.23
20/40/80	85	1.4	1.3	.29	-	85	1.4	1.4	.14	-
	turbulent kinetic energy (k)					dissipation rate of k (ϵ)				
grid	Rn	p	$\sigma_{p(x)}$	GCI^*	e_D^*	Rn	p	$\sigma_{p(x)}$	GCI^*	e_D^*
$n_3/n_2/n_1$	[%]			[%]	[%]	[%]			[%]	[%]
5/10/20	88	1.0	1.3	9.7	3.5	84	0.9	1.6	23.	5.8
10/20/40	90	1.1	1.1	3.2	1.0	88	1.0	1.2	5.1	2.0
20/40/80	90	1.2	1.0	.94	-	87	1.3	1.2	1.5	-

Table 5.4: Case B: Axisymmetric turbulent flow through a valve. Post-processing results. Numerical scheme: central differences for diffusive terms and SMART and PLDS for the momentum and turbulent quantities convective terms respectively. (For table description see section 5.5.1).

meshes. Furthermore, the e_D^* and the GCI^* have similar order of magnitude.

Case C involves, apart from the momentum, energy and continuity equations, the resolution of four additional convection diffusion equations to account for the mass fraction of the products and reactives of the combustion process. Therefore, the resulting algebraic equation system to be solved is highly complicated with a strong coupling between all the variables and with the algebraic coefficients highly dependent on the dependent variables.

The corresponding global estimators are given in tables 5.5 and 5.6. For all the situations, even for the most coarse set of solutions, the observed order of accuracy approximates the expected theoretical value. Most important discrepancies are found for the coarsest meshes, and for the finest meshes using the SMART schemes (where a degradation of the observed order of accuracy is detected, tending to 1). However, even in these cases, the observed order of accuracy approaches the expected p enough, so as to make the estimator GCI^* reliable. In fact, differences between e_D^* and the GCI^* are quite acceptable for the coarse meshes and tend to vanish for the finest meshes.

Case D is a two-dimensional heat transfer flow. The global estimators obtained from the post-processing are given in table 5.7. Reasonable values of observed accuracy are obtained and good accordance between the computational error estimator and the "exact" computational error is observed.

Global estimators like those presented in the previously referenced tables, are quite

	radial-velocity					axial-velocity				
grid	Rn	p	$\sigma_{p(x)}$	GCI^*	e_D^*	Rn	p	$\sigma_{p(x)}$	GCI^*	e_D^*
$n_3/n_2/n_1$	[%]			[%]	[%]	[%]			[%]	[%]
5/10/20	82	1.1	1.0	.67	.35	93	1.2	0.9	1.8	3.0
10/20/40	90	1.3	1.0	.18	.17	93	0.7	1.1	3.0	1.6
20/40/80	95	1.2	0.8	.09	.08	98	1.0	0.7	1.0	.86
40/80/160	98	1.1	0.5	.05	.04	98	1.0	0.5	.53	.44
80/160/320	97	1.0	0.6	.03	.02	98	1.0	0.5	.27	.23
	CH_4					O_2				
grid	Rn	p	$\sigma_{p(x)}$	GCI^*	e_D^*	Rn	p	$\sigma_{p(x)}$	GCI^*	e_D^*
$n_3/n_2/n_1$	[%]			[%]	[%]	[%]			[%]	[%]
5/10/20	100	0.7	0.8	11.	6.1	100	0.6	0.7	1.2	6.0
10/20/40	98	0.8	0.6	5.4	3.2	100	0.9	0.4	4.4	3.1
20/40/80	99	0.9	0.3	2.2	1.6	100	0.9	0.4	2.3	1.6
40/80/160	100	1.0	0.1	1.1	.84	99	1.0	0.2	1.0	.82
80/160/320	100	1.0	0.1	.53	.42	100	1.0	0.1	.55	.42
	CO_2					H_2O				
grid	Rn	p	$\sigma_{p(x)}$	GCI^*	e_D^*	Rn	p	$\sigma_{p(x)}$	GCI^*	e_D^*
$n_3/n_2/n_1$	[%]			[%]	[%]	[%]			[%]	[%]
5/10/20	93	0.4	0.7	17.	5.7	96	0.6	0.6	13.	6.5
10/20/40	95	0.8	0.3	4.6	3.0	99	0.9	0.4	4.4	3.4
20/40/80	100	0.9	0.3	2.0	1.5	100	1.0	0.3	2.1	1.7
40/80/160	100	0.9	0.2	.99	.79	100	1.0	0.2	1.1	.88
80/160/320	100	1.0	0.1	.51	.40	100	1.0	0.1	.55	.44
	temperature									
grid	Rn	p	$\sigma_{p(x)}$	GCI^*	e_D^*					
$n_3/n_2/n_1$	[%]			[%]	[%]					
5/10/20	93	0.7	0.6	6.7	4.4					
10/20/40	100	0.8	0.2	3.7	2.3					
20/40/80	100	0.9	0.1	1.6	1.2					
40/80/160	100	1.0	0.2	.77	.61					
80/160/320	100	1.0	0.1	.37	.31					

Table 5.5: Case C: Premixed methane/air laminar flat flame on a perforated burner. Post-processing results. Numerical scheme: UDS for convective terms and central differences for diffusive terms. (For table description see section 5.5.1).

	radial-velocity					axial-velocity				
grid	Rn	p	$\sigma_{p(x)}$	GCI^*	e_D^*	Rn	p	$\sigma_{p(x)}$	GCI^*	e_D^*
$n_3/n_2/n_1$	[%]			[%]	[%]	[%]			[%]	[%]
5/10/20	75	1.8	1.4	.27	.14	70	2.0	2.3	.78	.65
10/20/40	81	2.2	1.5	.05	.06	82	1.7	1.3	.34	.20
20/40/80	58	1.1	2.0	.06	.03	93	1.4	0.9	.11	.06
40/80/160	89	0.7	1.1	.04	.01	97	1.6	0.6	.03	.02
80/160/320	98	0.8	0.6	.01	-	95	1.4	0.9	.01	-
	CH_4					O_2				
grid	Rn	p	$\sigma_{p(x)}$	GCI^*	e_D^*	Rn	p	$\sigma_{p(x)}$	GCI^*	e_D^*
$n_3/n_2/n_1$	[%]			[%]	[%]	[%]			[%]	[%]
5/10/20	44	1.8	2.4	.91	.46	44	1.6	2.5	.95	.45
10/20/40	91	2.0	1.0	.15	.13	94	1.8	1.1	.18	.13
20/40/80	87	1.8	1.2	.05	.04	90	1.7	1.2	.05	.05
40/80/160	91	1.5	1.0	.02	.01	93	1.6	1.1	.02	.01
80/160/320	93	1.3	1.0	.01	-	91	1.4	1.2	.01	-
	CO_2					H_2O				
grid	Rn	p	$\sigma_{p(x)}$	GCI^*	e_D^*	Rn	p	$\sigma_{p(x)}$	GCI^*	e_D^*
$n_3/n_2/n_1$	[%]			[%]	[%]	[%]			[%]	[%]
5/10/20	49	0.8	2.4	2.4	.47	39	2.7	1.9	.43	.46
10/20/40	95	1.9	0.9	.16	.14	92	1.9	0.7	.18	.13
20/40/80	93	1.9	1.1	.05	.05	87	1.8	1.2	.05	.04
40/80/160	90	1.8	1.1	.02	.02	90	1.5	1.1	.02	.01
80/160/320	83	1.1	1.1	.02	-	93	1.2	1.0	.01	-
	temperature									
grid	Rn	p	$\sigma_{p(x)}$	GCI^*	e_D^*					
$n_3/n_2/n_1$	[%]			[%]	[%]					
5/10/20	77	0.8	1.3	1.9	.40					
10/20/40	85	1.8	0.9	.17	.13					
20/40/80	90	1.8	1.2	.05	.04					
40/80/160	87	1.5	1.1	.02	.01					
80/160/320	92	1.2	0.8	.01	-					

Table 5.6: Case C: Premixed methane/air laminar flat flame on a perforated burner. Post-processing results. Numerical scheme: SMART for convective terms and central differences for diffusive terms. (For table description see section 5.5.1).

UDS										
	x-velocity					y-velocity				
grid	Rn	p	$\sigma_{p(x)}$	GCI^*	e_D^*	Rn	p	$\sigma_{p(x)}$	GCI^*	e_D^*
$n_3/n_2/n_1$	[%]			[%]	[%]	[%]			[%]	[%]
2/4/8	77	2.5	2.3	.05	.06	70	1.6	1.5	.17	.09
4/8/16	77	1.8	1.7	.02	.03	80	1.2	1.4	.06	.05
8/16/32	68	1.3	1.6	.01	.01	77	1.2	1.4	.02	.02
	temperature									
grid	Rn	p	$\sigma_{p(x)}$	GCI^*	e_D^*					
$n_3/n_2/n_1$	[%]			[%]	[%]					
2/4/8	85	1.2	1.5	1.2	1.0					
4/8/16	85	1.2	1.1	.48	.58					
8/16/32	84	0.9	0.7	.41	.30					
SMART										
	x-velocity					y-velocity				
grid	Rn	p	$\sigma_{p(x)}$	GCI^*	e_D^*	Rn	p	$\sigma_{p(x)}$	GCI^*	e_D^*
$n_3/n_2/n_1$	[%]			[%]	[%]	[%]			[%]	[%]
2/4/8	73	2.1	2.6	.10	.05	64	1.9	1.9	.13	.05
4/8/16	76	2.3	1.9	.02	.01	71	2.0	1.6	.02	.01
8/16/32	80	1.9	1.2	.01	-	80	1.8	1.2	.01	-
	temperature									
grid	Rn	p	$\sigma_{p(x)}$	GCI^*	e_D^*					
$n_3/n_2/n_1$	[%]			[%]	[%]					
2/4/8	41	2.3	2.0	.11	.26					
4/8/16	65	1.4	1.7	.18	.10					
8/16/32	79	1.7	1.1	.03	-					

Table 5.7: Case D: Heat transfer from an isothermal cylinder enclosed by a square duct. Post-processing results. Numerical scheme: UDS and SMART for convective terms and central differences for diffusive terms. (For table description see section 5.5.1).

promising in terms of reporting purposes because they can be reproduced by different authors, and they can be reported in a compact manner. When these estimators are obtained from the procedure described in this paper, they arise from a statistical treatment of local estimators. These estimators made up a large amount of data which is difficult to be reported. However, this information is very useful for the user of the computational code, because it makes it possible to find out local source of errors, such as zones with insufficient mesh concentration or problems with the boundary conditions.

As an example, the local estimators corresponding to the solution of case D with the grid $n = 32$, and the numerical scheme UDS, are shown in Fig. 5.5. For each one of the dependent variables of the case (x-velocity, y-velocity and temperature), the isolines, the post-processing grid ($n = 8$), the Richardson nodes, the estimated order of accuracy $p(\mathbf{x})$, the estimated normalized local computational error $GCI^*(\mathbf{x})$, and the "exact" normalized local computational error $e^*_D(\mathbf{x})$ are given. In the maps of local p and local GCI^*, the zones corresponding to non-Richardson nodes (all of them oscillatory nodes) and where the post-processing procedure cannot be performed, have been blanked. As expected, local observed p at a given point of the domain can have quite different values from one dependent variable to another, depending on the local nature of the corresponding physical equation. Furthermore, obviously one point in the domain may not fulfill the conditions required for the Richardson nodes when analyzing one of the variables, while being a Richardson node when analyzing the other dependent variables. On the other hand, it can been observed that the maps of $GCI^*(\mathbf{x})$ predict the corresponding maps of "exact" normalized absolute computational error quite well. Therefore, these kind of maps are quite useful when analyzing a new problem to be solved by means of computational techniques, giving criteria to the code user about how and where the grid has to be intensified so as to improve the quality of the computational solution.

5.5.3 Further discussion

Results discussed in the previous section show that the estimated discretization error band obtained from the post-processing procedure reproduces the "exact" absolute computational error (obtained numerically as indicated in section 5.5.1) quite well in all the tested problems. All these results give confidence about the certainty of the estimators. However, the estimated discretization error is compared to a value (the "exact" computational error) which may not be free from computational error. Therefore, some doubts about the certainty of the estimators can still remain.

So as to go a step further towards assessing the credibility of the estimator of the discretization error, in this subsection the post-processed results of the numerical solution of a case with analytical solution will be shown. These results will be compared to the exact absolute computational error (take note that now the word exact is not

Figure 5.5: Case D: Heat transfer from an isothermal cylinder enclosed by a square duct. Post-processing results. Local estimators of the solution with the grid $n = 32$ (post-processing grid $n = 8$) and the numerical scheme UDS.

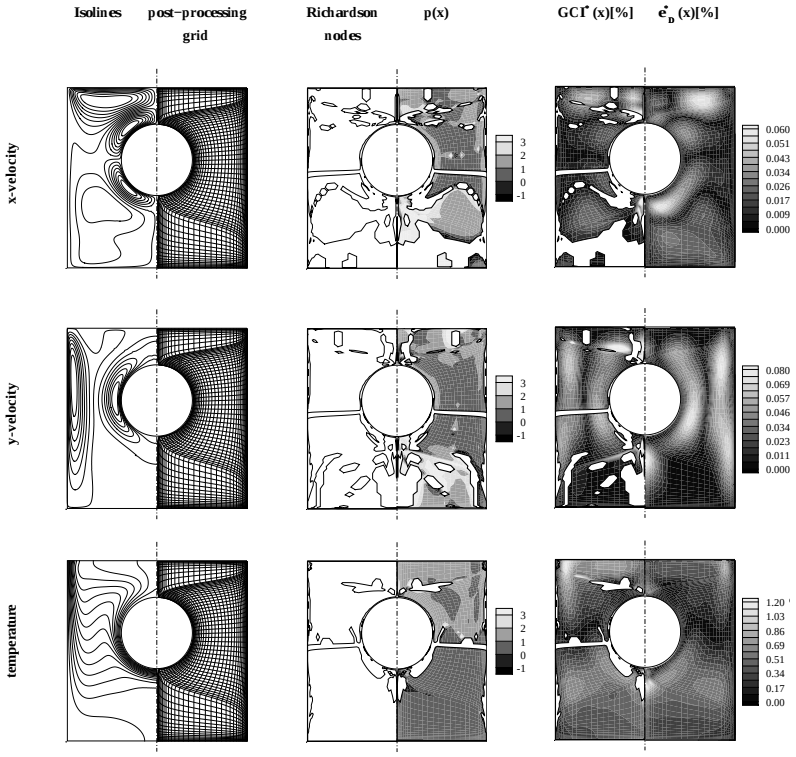

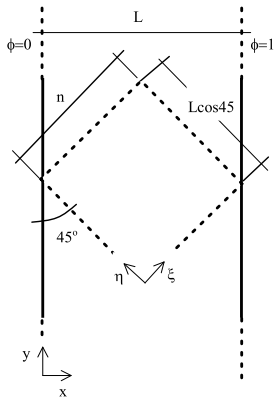

Figure 5.6: Case with analytical solution: One dimensional steady state convection-diffusion process without source term, with constant transport properties and with Dirichlet boundary conditions. Computational domain: square domain with an inclination of 45^o and discretized by means of a uniform mesh of $n * n$ control volumes.

written within quotation marks because it is obtained from the analytical solution).

The evaluated case consists of the steady state convection-diffusion process of a variable $\phi(x, y)$ without source term and constant transport properties within a domain with infinite height (y dimension), a width L (x dimension), and with the Dirichlet boundary conditions in the x direction $\phi(0, y) = \phi_0 = 0$ and $\phi(L, y) = \phi_L = 1$, see Fig. 5.6. In such conditions the convection-diffusion equation yields to a one-dimensional equation (x dependent) with the well known analytical solution $\phi(x) = (1 - e^{Pe\frac{x}{L}})/(1 - e^{Pe})$, where Pe is the Peclet number (ratio between the convective and diffusive coefficients). For more details see [9].

The computational domain is a square domain inclined at an angle of 45^o with respect to the x direction, with one vertex at $x = 0$ and the opposite vertex at $x = L$. Dirichlet boundary conditions have been fixed according to the analytical solution. A uniform mesh of $n * n$ control volumes is used. Both calculations using the UDS and SMART schemes for the convective terms have been performed, while central differences have always been used for the diffusive terms.

Six levels of h-refinement have been solved ($n = 10, 20, 40, 80$, 160 and 320). Results of the post-processing of these results are given in table 5.8 for two different Pe numbers and the two numerical schemes used for the convective terms. Other Pe numbers not presented herewith have also been studied. The Grid Convergence Index GCI and the exact absolute discretization error e_D have been normalized using

		UDS					SMART				
grid	Pe	Rn	p	$\sigma_{p(x)}$	GCI^*	e^*_D	Rn	p	$\sigma_{p(x)}$	GCI^*	e^*_D
$n_3/n_2/n_1$		[%]			[%]	[%]	[%]			[%]	[%]
10/20/40		89	1.1	1.1	1.2	1.0	85	1.8	0.9	.48	.32
20/40/80	1	94	1.0	0.8	.69	.52	96	1.8	1.0	.12	.09
40/80/160		97	1.0	0.6	.35	.26	99	1.9	0.7	.03	.02
80/160/320		98	1.0	0.5	.17	.13	100	1.9	0.5	.01	.01
10/20/40		99	0.8	0.4	17.	12.	83	1.8	1.4	1.8	.80
20/40/80	10	99	0.9	0.3	8.7	6.5	89	1.8	0.6	.42	.21
40/80/160		100	0.9	0.2	4.4	3.3	97	1.8	0.7	.09	.05
80/160/320		100	1.0	0.2	2.2	1.7	99	1.9	0.4	.02	.01

Table 5.8: Case with analytical solution: One dimensional steady state convection-diffusion process without source term, with constant transport properties and with Dirichlet boundary conditions, $Pe = 1$ and $Pe = 10$. Post-processing results. (For table description see section 5.5.1).

a reference value of $\Delta\phi = 0.01(\phi_L - \phi_0)$. As it is shown, the GCI has predicted the exact absolute discretization error for all the studied situations quite well.

5.6 Conclusions

This work addresses the verification process of finite volume numerical solutions. Even when a code has been previously submitted to a credibility test by comparison with a set of either previously accepted simulations or experimental data, the credibility of the results of new problems or situations is not assessed. Therefore, specific credibility tests must be carried out before the solution can be accepted. The credibility tests encompass the study of the physical model used to represent the physical phenomena, the verification of the numerical solution (accuracy of the computational model) and the validation by comparison to experimental results.

A post-processing tool for the study of the discretization errors (verification process) based on the generalized Richardson extrapolation and on the concept of grid convergence index GCI has been presented. This tool not only estimates an error band where the grid-independent solution is expected to be contained, but also the order of accuracy of the numerical solution (observed p). Both local and global estimators are computed. While local estimators are a good tool for the code user in order to improve the quality of the numerical solutions, global error estimators seem easier to be used and reproduced for different authors in the final reporting of the

results.

The numerical results of different heat transfer and fluid flow problems involving different phenomena (laminar flow, turbulent flow and reactive flow), adopting different meshes (Cartesian grids in a staggered arrangement, axisymmetric grids in a staggered arrangement, and body fitted coordinates in a non-staggered arrangement) and different numerical schemes have been post processed. The obtained global error band estimators have been given for all of them. Local absolute error estimators of one of the post processed results have also been shown. The certainty of the error band estimators has been checked comparing its value to the "exact" absolute error of the numerical solutions always obtaining very reasonable values. The post-processing results have been discussed in detail in order to give criteria about the credibility of the numerical solutions. Although the error estimators obtained with the post-processing procedure here described have been shown to be quite reliable for all the studied cases, whether these estimators are reliable or not in other kind of flows, will require further research.

5.7 Acknowledgments

This work has been financially supported by the Comisión Interministerial de Ciencia y Tecnología, Spain (project TIC1999-0770), and by the Comissionat per Universitats i Recerca de la Generalitat de Catalunya. Detailed comments and suggestions of the reviewers of the Journal of Fluids Engineering have been introduced in the text improving some technical aspects and making the paper more comprehensible.

References

[1] Not known. AIAA guide for the verification and validation of computational fluid dynamics simulations, 1998.

[2] Journal of Fluids Engineering. Journal of fluids engineering editorial policy. statement on the control of numerical accuracy, editorial. *Journal of Fluids Engineering*, 115:339–342, 1993.

[3] AIAA Journal. Special section: credible computational fluid dynamics simulations. *AIAA Journal*, 36:665–764, 1998.

[4] P.J. Roache. Verification of codes and calculations. *AIAA Journal*, 36(5):696–702, 1998.

[5] I. Celik and Vei-Ming Zhang. Calculation of numerical uncertainty using richardson extrapolation: application to some simple turbulent flow calculations. *Journal of Fluids Engineering*, 117:439–445, 1995.

[6] C.D. Pérez-Segarra, A. Oliva, M. Costa, and F. Escanes. Numerical experiments in turbulent natural and mixed convection in internal flows. *International Journal for Numerical Methods for Heat and Fluid Flow*, 5(1):13–33, 1995.

[7] R. Cònsul, C.D. Pérez-Segarra, J. Cadafalch, M. Soria, and A. Oliva. Numerical analysis of laminar flames using the domain decomposition method. In *Proceedings of the Fourth European Computational Fluid Dynamics Conference (ECCOMAS CFD)*, volume 1.2, pages 996–1001, 1998.

[8] P.J. Roache. Perspective: a method for uniform reporting of grid refinement studies. *Journal of Fluids Engineering*, 116:405–413, 1994.

[9] J. Cadafalch, A. Oliva, C.D. Pérez-Segarra, M. Costa, and J. Salom. Comparative study of conservative and nonconservative interpolation schemes for the domain decomposition method on laminar incompressible flows. *Numerical Heat Transfer, Part B*, 35(1):65–84, 1999.

[10] J. Cadafalch, C.D. Pérez-Segarra, M. Sòria, and A. Oliva. Fully conservative multiblock method for the resolution of turbulent incompressible flows. In *Proceedings of the Fourth European Computational Fluid Dynamics Conference (ECCOMAS CFD)*, volume 1.2, pages 1234–1239, 1998.

[11] C.D. Pérez-Segarra, A. Oliva, and R. Cònsul. Analysis of some numerical aspects in the solution of the navier-stokes equations using non-orthogonal collocated finite-volume methods. In *Proceedings of the Second European Congress on Computational Methods in Applied Sciences and Engineering (ECCOMAS)*, pages 505–511, 1996.

[12] I. Demirdzic, Z. Lilek, and M. Peric. Fluid flow and heat transfer test problems for non-orthogonal grids: bench-mark solutions. *International Journal for Numerical Methods in Fluids*, 15:329–354, 1992.

[13] C.D. Pérez-Segarra, J. Cadafalch, J. Rigola, and A. Oliva. Numerical study of turbulent fluid flow through valves. In *Proceedings of the 1999 International Conference on Compressors and Their Systems*, pages 399–408, 1999.

[14] L.M.T. Somers. *The simulation of flat flames with detailed and reduced chemical models*. PhD thesis, Technical University of Eindhoven, 1994.

[15] M. Soria, J. Mora, C. Lifante, and C. Farré. Algoritmos paralelos para simulaciones numéricas en dinámica de fluidos y transferencia de calor utilizando redes de ordenadores personales. In *Anales de Ingeniería Mecánica (Revista de la Asociación Española de Ingeniería Mecánica, Año 12)*, volume 3, pages 1607–1612, 2000.